Inhibition of the p110α isoform of PI 3-kinase stimulates nonfunctional tumor angiogenesis

Adriana Soler,[1] Helena Serra,[1] Wayne Pearce,[3] Ana Angulo,[1]
Julie Guillermet-Guibert,[3] Lori S. Friedman,[4] Francesc Viñals,[2]
Holger Gerhardt,[5] Oriol Casanovas,[2] Mariona Graupera,[1]
and Bart Vanhaesebroeck[3]

[1]Vascular Signaling Laboratory; and [2]Translational Research Laboratory, Catalan Institute of Oncology, Institut d'Investigació
 Biomèdica de Bellvitge (IDIBELL), 08907 L'Hospitalet de Llobregat, Barcelona, Spain
[3]Centre for Cell Signaling, Barts Cancer Institute, Queen Mary University of London, Charterhouse Square, London
 EC1M 6BQ, England UK
[4]Department of Cancer Signaling, Genentech, Inc., South San Francisco, CA
[5]Vascular Biology Laboratory, London Research Institute-Cancer Research UK, London WC2A 3LY, England UK

Understanding the direct, tumor cell–intrinsic effects of PI 3-kinase (PI3K) has been a key focus of research to date. Here, we report that cancer cell–extrinsic PI3K activity, mediated by the p110α isoform of PI3K, contributes in an unexpected way to tumor angiogenesis. In syngeneic mouse models, inactivation of stromal p110α led to increased vascular density, reduced vessel size, and altered pericyte coverage. This increased vascularity lacked functionality, correlating with enhanced tumor hypoxia and necrosis, and reduced tumor growth. The role of p110α in tumor angiogenesis is multifactorial, and includes regulation of proliferation and DLL4 expression in endothelial cells. p110α in the tumor stroma is thus a regulator of vessel formation, with p110α inactivation giving rise to nonfunctional angiogenesis, which can stunt tumor growth. This type of vascular aberration differs from vascular endothelial growth factor–centered antiangiogenesis therapies, which mainly lead to vascular pruning. Inhibition of p110α may thus offer a new antiangiogenic therapeutic opportunity in cancer.

CORRESPONDENCE
Mariona Graupera:
mgraupera@idibell.cat

Abbreviations used: EC, endothelial cell; KI, knock-in; mLEC, mouse lung EC; PI3K, phosphoinositide 3-kinase; TUNEL, terminal deoxynucleotidyl transferase (TdT)–mediated dUTP nick end labeling; VEGF, vascular endothelial growth factor.

Constitutive activation of the PI3K pathway is very common in cancer, and PI3K inhibitors are currently progressing through oncology trials (Rodon et al., 2013). At present, the role of PI3K in the tumor microenvironment, such as in cancer-associated fibroblasts, endothelial cells (ECs), mural cells, and immune cells, is largely unexplored. With the exception of white blood cells, where p110γ and p110δ both play important roles (including in cancer; p110γ; Schmid et al., 2011), the ubiquitously expressed p110α is likely to be a critical PI3K isoform in nonleukocyte stromal cell types, based on the notion that p110α plays a nonredundant key role in vascular development (Lelievre et al., 2005; Graupera et al., 2008) and fibroblast proliferation (Foukas et al., 2006; Zhao et al., 2006). However, the role of p110α in the tumor stroma

is unknown. To assess the importance of the p110α PI3K axis in the cancer stromal compartment, we manipulated this pathway in syngeneic mouse cancer models.

RESULTS AND DISCUSSION
Systemic pharmacological blockade of p110α and p110δ in mice leads to decreased B16F1 melanoma growth and aberrant angiogenesis
In vitro treatment of B16F1 cells with PI3Ki-A/D, a small molecule inhibitor with selectivity for p110α and p110δ (Edgar et al., 2010), reduced Akt phosphorylation (Fig. 1 A), without affecting cell proliferation (Fig. 1 B) or survival (Fig. 1 C). This compound also reduced in vitro production of vascular endothelial growth factor (VEGF)

M. Graupera and B. Vanhaesebroeck contributed equally to this paper.
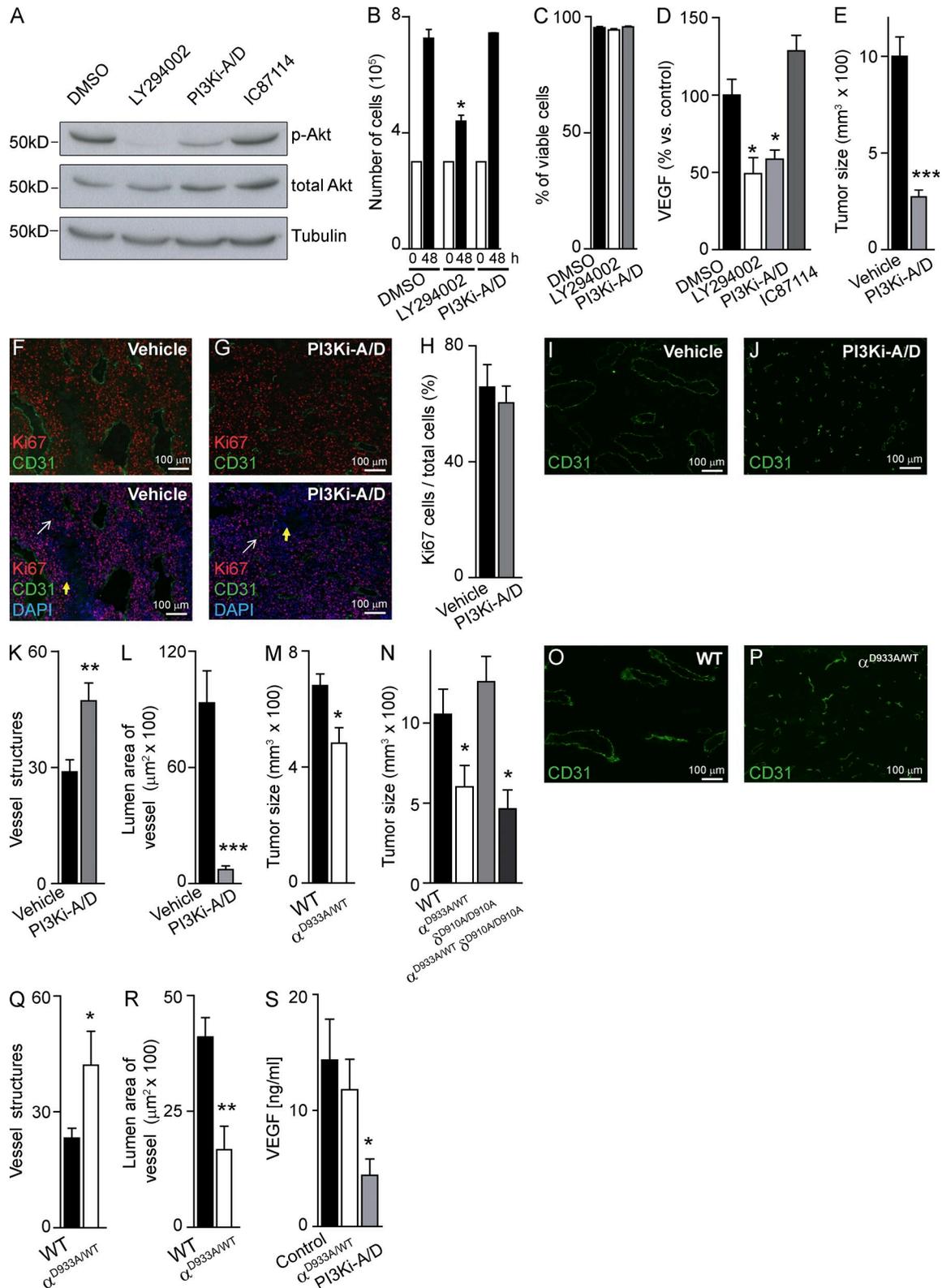
Figure 1. p110α inhibition reduces in vivo growth of B16F1 melanoma tumors. (A) B16F1 cells were treated for 1 h with compounds or vehicle, followed by immunoblotting of total cell lysate using the indicated antibodies (*n* = 3). (B) In vitro proliferation (*n* = 3) and (C) cell viability (*n* = 3) of B16F1 cells after 48-h in vitro treatment with vehicle, LY294002, or PI3Ki-A/D. (D) B16F1 cells were treated with test compounds or vehicle, followed by quantitation of VEGF secreted into the culture medium (*n* = 4). (E) Size of B16F1 tumors treated for 16 d with vehicle (*n* = 10) or PI3Ki-A/D

by B16F1 cells (Fig. 1 D). In mice, administration of PI3Ki-A/D severely blunted B16F1 tumor growth (Fig. 1 E) without affecting in vivo tumor cell proliferation (Fig. 1, F–H). PI3Ki-A/D–treated tumors had increased numbers of CD31-positive blood vessels (Fig. 1 I-K) with reduced size, compared with vehicle-treated mice (Fig. 1, I, J, and L). This induction by PI3Ki-A/D of aberrant angiogenesis, with enhanced vessel density and reduced vessel caliber, is likely to contribute to the observed reduction in B16F1 tumor growth in vivo.

Stromal inhibition of p110α reduces B16F1 tumor growth and increases the density of smaller blood vessels

To investigate the impact of p110α inactivation in the stroma only, we inoculated B16F1 cells in mice heterozygous for the kinase-dead p110α[D933A] knock-in (KI) allele (Foukas et al., 2006), further referred to as p110α[D933A/WT] mice. p110α[D933A/WT] mice exhibit delayed vascular development, but their vascular plexuses are indistinguishable from WT littermates upon reaching adulthood (unpublished data). We also inoculated B16F1 cells in p110δ[D910A/D910A] KI mice (Okkenhaug et al., 2002) and in p110α[D933A/WT]/p110δ[D910A/D910A] compound KI mice, to assess the possible involvement of p110δ reactivity of PI3Ki-A/D in the biological actions of this compound. Growth of B16F1 tumors was significantly reduced in p110α[D933A/WT] mice (Fig. 1 M), to a similar extent as observed upon inoculation in p110α[D933A/WT]/p110δ[D910A/D910A] KI mice (Fig. 1 N). Tumor growth was unaffected in p110δ[D910A/D910A] KI mice (Fig. 1 N), suggesting that, under the experimental conditions tested, p110δ inactivation in the tumor stroma, on its own or in combination with partial inactivation of p110α, does not affect B16F1 tumor growth. These observations further imply that the antitumor effect of PI3Ki-A/D is mainly a result of inhibition of p110α.

The number of tumor blood vessels was increased in p110α[D933A/WT] mice compared with WT mice (Fig. 1, O–Q), with a reduction in vessel luminal area (Fig. 1 R). The PI3Ki-A/D–induced reduction in vessel area and tumor growth was stronger than upon stromal inactivation of p110α (compare Fig. 1 L to Fig. 1 R, and Fig. 1 E to Fig. 1 M), possibly related to the reduction in intratumoral VEGF levels upon pharmacological intervention (Fig. 1 S). These data suggest that both stromal and cancer-intrinsic blockade of p110α is required for maximal impact on tumor growth and angiogenesis. It is important to keep in mind, however, that p110α activity is only reduced by 50% in the p110α[D933A/WT] mice (Graupera et al., 2008), whereas PI3Ki-A/D has the capacity to fully block p110α signaling, in both the tumor and the stroma.

p110α inactivation reduces mural cell coverage of B16F1 tumor blood vessels

Compared with B16F1 tumors in WT mice, tumor vessels in p110α[D933A/WT] mice showed a clear trend for decreased positivity for the mural cell marker α-SMA (Fig. 2, A, B, and G), with enhanced expression of the pericyte markers desmin (Fig. 2, C, D, and H) and NG2 (Fig. 2, E, F, and I). PI3Ki-A/D had a similar impact (Fig. 2, G–I). In normal tissue, α-SMA is expressed in the smooth muscle cells of large vessels and rarely expressed in capillary pericytes. In cancer, however, capillaries are often α-SMA⁺. Conversely, desmin and NG2 are markers of normal pericytes, but show a more variable expression in tumor-associated pericytes (Armulik et al., 2011). This diminished positivity of α-SMA but strong expression of desmin and NG2 suggests a more mature/quiescent pericyte phenotype of the PI3K-inhibited vessels. It remains possible, however, that the observed pericyte alterations upon p110α inhibition do not have a functional role, but simply correlate with the reduced vessel caliber.

p110α inhibition also induces aberrant angiogenesis in the CMT19T carcinoma tumor model

Genetic (Fig. 2 J) or pharmacological (Fig. 2 K) inactivation of p110α significantly reduced intradermal tumor growth of CMT19T lung carcinoma cells in syngeneic mice. The number of blood vessels in these tumors was substantially increased upon stromal inhibition of p110α (Fig. 2, L–N), with a similar (but statistically not significant) trend upon treatment with PI3Ki-A/D (Fig. 2, P–R). The luminal area of the vessels was decreased upon genetic or pharmacological inhibition of p110α (Fig. 2 O and S). p110α inhibition in CMT19T tumors also recapitulated the altered pericyte phenotype observed in the B16F1 model, with reduced α-SMA staining (Fig. 2 T) and increased expression of desmin (Fig. 2 U).

Our observations are in line with the inability of mice with EC-specific loss of the p85 PI3K regulatory subunits to form large vessels (Yuan et al., 2008). Analogous observations have been made in mice with altered activity of Akt, a key downstream target of p110α. Indeed, tumor vascular density is increased in Akt1 KO mice (Chen et al., 2005) and vessel size is increased in mice which express a constitutively active Akt1 transgene (Phung et al., 2006). Together, these data establish a p85/p110α/Akt1 signaling axis in tumor angiogenesis.

p110α inhibition reduces proliferation of tumor–associated ECs

Inactivation of p110α in the tumor stroma reduced PI3K signaling in ECs in vivo, as indicated by a decrease in the

---

(n = 10). (F and G) Sections of vehicle- or PI3Ki-A/D–treated B16F1 tumors stained with the indicated antibodies. White and yellow arrows indicate proliferating and nonproliferating cells, respectively. (H) Quantification of in vivo–proliferating B16F1cells. (I and J) CD31-stained sections of vehicle- or PI3Ki-A/D–treated B16F1 tumors. (K) Quantification of vessel structures and (L) lumen area of vessels of mice treated with vehicle (n = 10) or PI3Ki-A/D (n = 8). (M) Size of tumors inoculated in WT (n = 14) or p110α[D933A/WT] (n = 11) mice. (N) Size of tumors inoculated in WT (n = 7), p110α[D933A/WT] (n = 5), p110δ[D910A/D910A] (n = 6), or p110α[D933A/WT]/p110δ[D910A/D910A] (n = 4) mice. (O and P) CD31-stained sections of tumors inoculated in WT or p110α[D933A/WT] mice. (Q) Quantification of vessel structures and (R) lumen area of the vessels in WT (n = 5) or p110α[D933A/WT] (n = 5) mice. (S) Quantitation of VEGF content in tumors in control (n = 11), PI3Ki-A/D-treated (n = 5), or p110α[D933A/WT] (n = 8) mice.

number of ECs staining positive for phospho-Ser240/244-S6, a marker of PI3K pathway activation (Fig. 3, A, B, and G).

Genetic or pharmacological inhibition of p110α led to a reduction in EC proliferation (Fig. 3 C, D and H), with no

evidence for an impact on EC survival (Fig. 3, E, F, and I). Reduced proliferation of tumor-associated ECs upon p110α inhibition might contribute to diminished vessel size. During developmental angiogenesis, partial inactivation of p110α
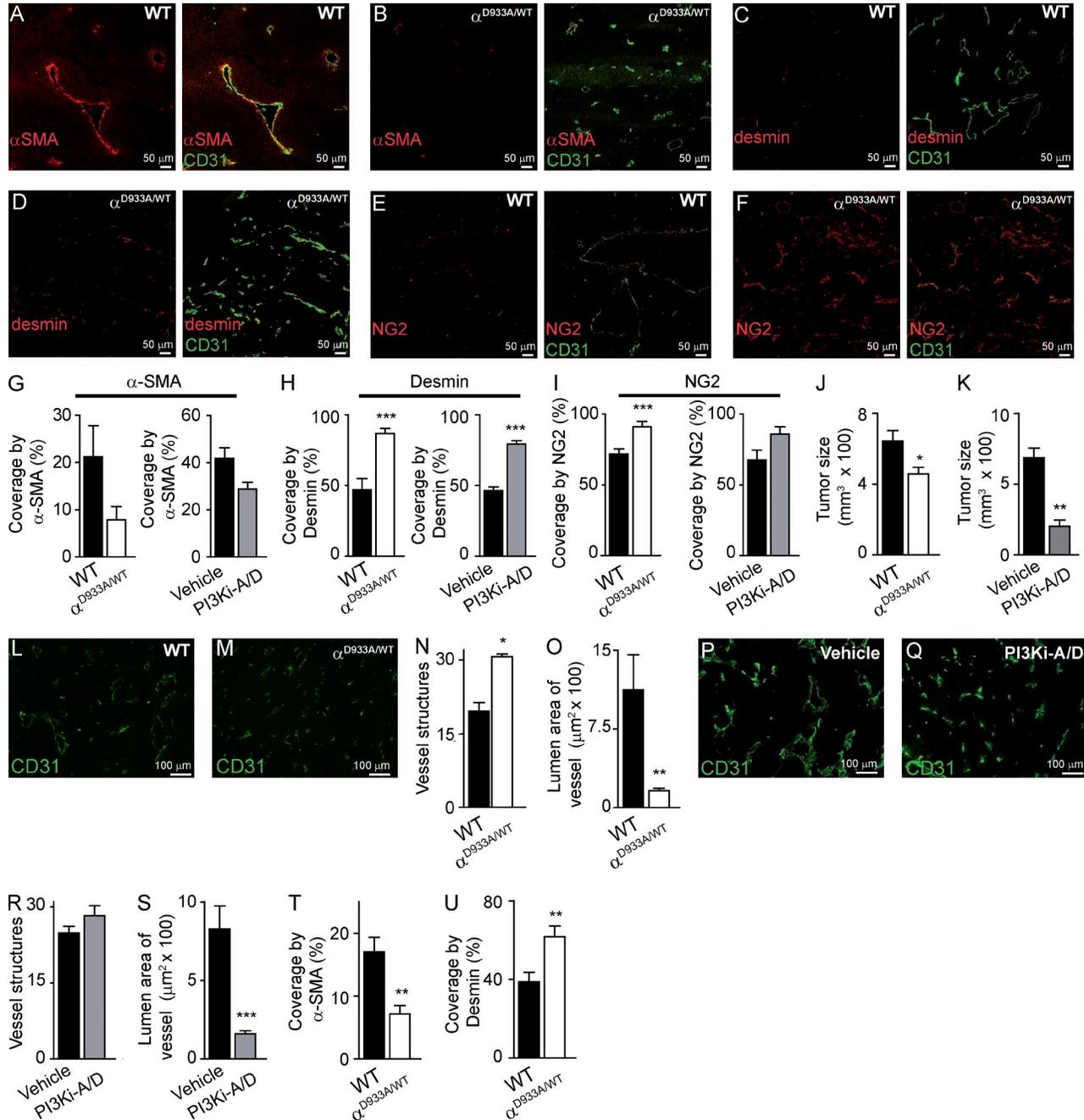
Figure 2. p110α inhibition alters mural cell coverage of vessels in B16F1 and CMT19T tumors. (A–F) Sections of B16F1 tumors stained for CD31 and α-SMA (A and B), desmin (C and D), or NG2 (E and F). (G–I) Quantification of vessels positive for α-SMA (G), desmin (H), and NG2 (I) in tumors implanted in WT ($n = 5$) or p110α$^{D933A/WT}$ ($n = 5$) mice and in tumors treated with vehicle ($n = 6$) or PI3Ki-A/D ($n = 6$). (J and K) Size of CMT19T tumors inoculated in WT ($n = 18$) or p110α$^{D933A/WT}$ ($n = 18$) mice (J), and of tumors treated with vehicle ($n = 9$) or PI3Ki-A/D ($n = 10$; K). (L, M, P, and Q) CD31-stained sections of tumors inoculated in WT or p110α$^{D933A/WT}$ mice (L and M) and of tumors of vehicle- or PI3Ki-A/D–treated mice (P and Q). (N and R) Quantification of vessel structures in WT ($n = 5$) or p110α$^{D933A/WT}$ ($n = 4$) mice (N) and of mice treated with vehicle ($n = 9$) or PI3Ki-A/D ($n = 9$; R). (O and S) Quantification of lumen area of vessels in CMT19T tumors in WT ($n = 5$) or p110α$^{D933A/WT}$ ($n = 4$) mice (O) or from mice treated with vehicle ($n = 9$) or PI3Ki-A/D ($n = 9$; S). (T and U) Quantification of α-SMA–positive (T) and desmin-positive vessels (U) in tumors implanted in WT ($n = 10$) or p110α$^{D933A/WT}$ ($n = 7$) mice.

Figure 3. p110α inhibition results in reduced PI3K signaling and proliferation in B16F1 tumor–associated ECs. (A and B) Sections of tumors stained for CD31 and pSer240/244-S6. White arrowheads indicate ECs that are positive for pSer240/244-S6. (C and D) Sections of tumors stained for CD31, KI67, and DAPI. Yellow arrows indicate Ki67-positive ECs. (E and F) Section of tumors stained for CD31 and TUNEL. Boxed regions in E and F are shown in the bottom images. White arrows indicate TUNEL-positive ECs. (G) Quantification of pSer240/244-S6–positive ECs relative to the total numbers of ECs per vessel in tumors in WT (*n* = 10) or p110α$^{D933A/WT}$ (*n* = 28) mice. (H) Quantification of Ki67-positive ECs per total number of ECs per section area in tumors in WT (*n* = 4) or p110α$^{D933A/WT}$ (*n* = 5) mice and in tumors treated with vehicle (*n* = 5) or PI3Ki-A/D (*n* = 6). (I) Quantification of the TUNEL-positive ECs per total number of ECs per section area in tumors in WT (*n* = 4) or p110α$^{D933A/WT}$ (*n* = 5) mice and in tumors treated with vehicle (*n* = 6) or PI3Ki-A/D (*n* = 6).

does not affect EC proliferation (Graupera et al., 2008). In the tumor microenvironment, however, ECs may become sensitized, given that the vessels in p110α$^{D933A/WT}$ mice become aberrant upon tumor cell inoculation, i.e., under stress. This difference in impact on angiogenesis under steady-state and stressed conditions is not unique to p110α, but is also observed in many other mouse mutants, including Akt1 and Ang2 mutant mice, which show vascular alterations in tumors but not in developmental angiogenesis (Chen et al., 2005; Nasarre et al., 2009). Of note, changes in pericytes can also attenuate EC proliferation (Hirschi and D'Amore, 1997) and it is possible that altered p110α signaling in pericytes leads to aberrant EC–pericyte cross-talk.

We cannot rule out that reduced EC migration upon p110α inhibition (Graupera et al., 2008; Herbert et al., 2009) may also contribute to the angiogenesis phenotype observed in tumors. Indeed, reducing EC motility may force ECs to stay put, which could increase pericyte cell coverage and induce phenotypic changes in these cells, as observed in tissues with a slow vascular turnover (Díaz-Flores et al., 2009).

p110α inhibition reduces tumor blood vessel functionality

To understand the paradox of increased vessel density and decreased tumor growth upon p110α inactivation, we tested vessel functionality in B16F1 tumors. Tumors in p110α$^{D933A/WT}$ mice displayed enhanced hypoxia (Fig. 4, A, B, and G) and an overall increased tumor cell death (Fig. 4, C, D, and H). Likewise, PI3Ki-A/D treatment also led to increased hypoxia and necrosis in B16F1 tumors (Fig. 4, G and H). Given that B16F1 cells are not sensitive to the direct antiproliferative/cytotoxic action of PI3K inhibition in vitro (Fig. 1, B and C), these observations suggest that the cell death observed in tumors is a consequence of unfavorable stromal conditions induced by PI3K inhibition. Tumor vessel perfusion, as measured by monitoring lectin positivity of vessels after intravenous administration of fluorescent lectin, was reduced in p110α$^{D933A/WT}$ mice (Fig. 4, E, F, and I). Together, these data show that reduced p110α activity in the tumor stroma led to hypoperfused supernumerary vessels, correlating with impaired oxygenation, enhanced tumor cell death, and reduced tumor growth.
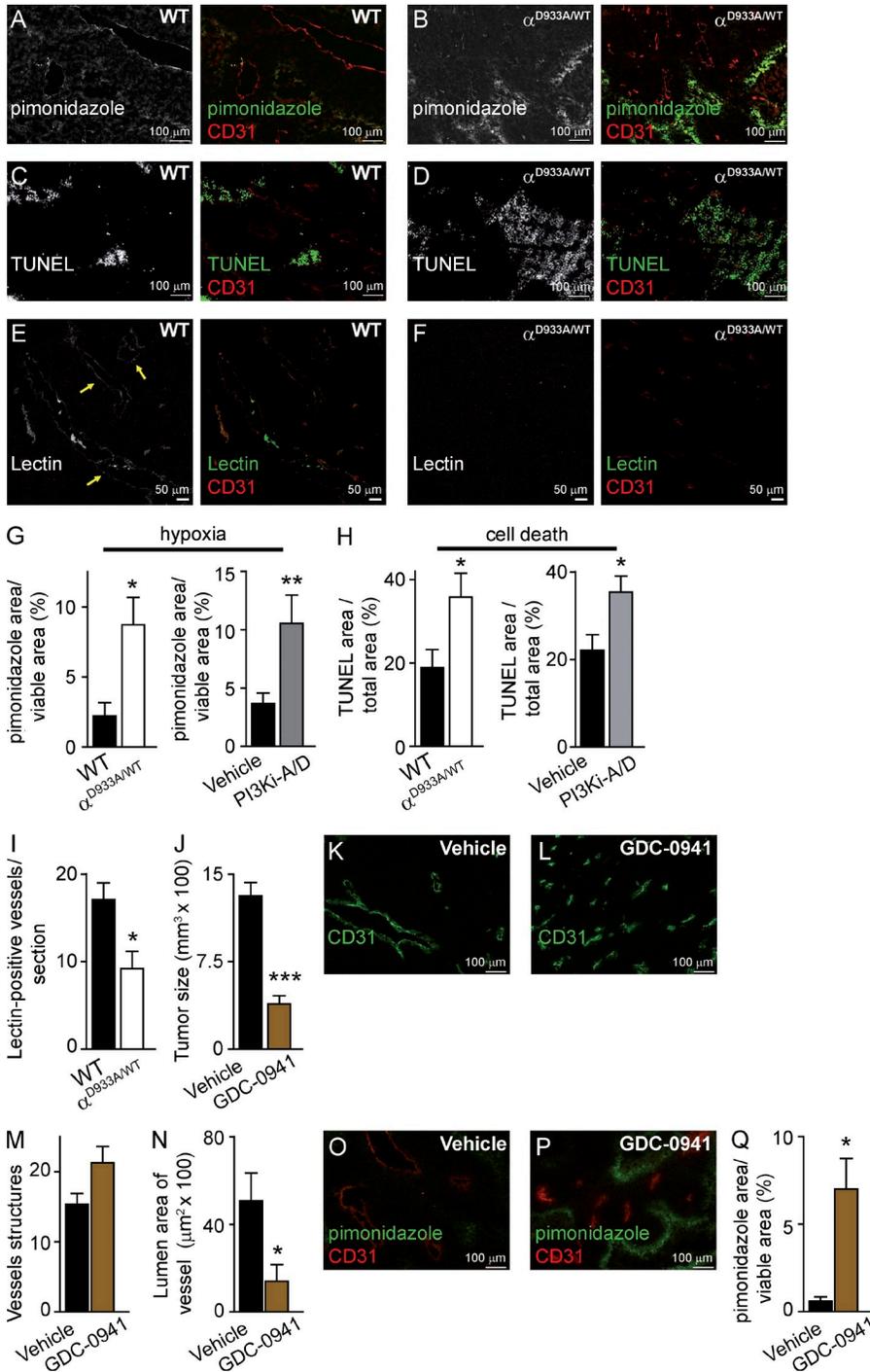
Figure 4. p110α inhibition increases B16F1 tumor hypoxia and necrosis and reduces vessel perfusion. (A–D) Sections of tumors stained for CD31 and pimonidazole (A and B) or by TUNEL (C and D). (E and F) Sections of tumors stained for lectin and CD31. Yellow arrows indicate perfused vessels. (G) Quantification of the hypoxic area of tumors implanted in WT ($n = 6$) or p110α$^{D933A/WT}$ ($n = 7$) mice and in tumors treated with vehicle ($n = 22$) or PI3Ki-A/D ($n = 20$). (H) Quantification of the necrotic and apoptotic area in tumors implanted in WT ($n = 5$) or p110α$^{D933A/WT}$ ($n = 5$) mice and in tumors treated with vehicle ($n = 10$) or PI3Ki-A/D ($n = 9$). (I) Quantification of perfused vessels (lectin-positive vessels) within the viable area in tumors implanted in WT ($n = 3$) or p110α$^{D933A/WT}$ ($n = 3$) mice. (J) Size of tumors treated with vehicle or GDC-0941 ($n \geq 8$). (K and L) Sections of tumors stained for CD31 after treatment with vehicle or GDC-0941. (M) Quantification of vessel structures of mice treated with vehicle ($n = 9$) or GDC-0941 ($n = 6$). (N) Quantification of lumen area of vessels in tumors treated with vehicle ($n = 9$) or GDC-0941 ($n = 6$). (O and P) Sections of tumors stained for CD31 and pimonidazole after treatment with vehicle or GDC-0941. (Q) Quantification of the hypoxic area relative to the viable area of tumors treated with vehicle ($n = 9$) or GDC-0941 ($n = 6$).

Our findings differ from previously published studies (Qayum et al., 2009, 2012) which showed that pan-class I PI3K inhibitors (PI-103 and GDC-0941) induce enhanced tumor vascular flow, perfusion, and oxygenation in human xenograft cancer models, with no differences in tumor growth, vessel density, or size. To clarify this discrepancy, we tested the impact of GDC-0941 (which blocks p110α, p110β, p110δ, and p110γ) on B16F1 tumors. GDC-0941 was found to inhibit tumor growth (Fig. 4 J) to a similar extent as PI3Ki-A/D

(Fig. 1 E). Pan-class I PI3K inhibition also resulted in increased vascular density and reduced vessel size (Fig. 4, K–N) and increased tumor hypoxia (Fig. 4, O–Q), suggesting a nonfunctional vasculature. The reason for the differences between our data and that of Qayum et al. (2009, 2012) is unclear at the moment, but may relate to the use of syngeneic versus xenograft mouse models. Our data further indicate that p110β and p110γ are not involved in B16F1 tumor growth and angiogenesis, given that treatment with PI3Ki-A/D (p110α/δ

inhibitor) and GDC-0941 (p110α/β/γ/δ inhibitor) gave rise to a similar reduction in tumor growth and a similar tumor vasculature phenotype.

p110α inhibition results in reduced DLL4 expression in ECs
Our data show that blocking p110α supports nonfunctional angiogenesis, a phenotype highly reminiscent of that observed upon inhibition of the Notch ligand DLL4 (Noguera-Troise et al., 2006; Ridgway et al., 2006). The PI3K pathway has been documented to positively regulate DLL4 production (Liu et al., 2003) and the activity of γ-secretase which proteolytically cleaves Notch (Takeshita et al., 2007). Conversely, Notch signaling stimulates Akt phosphorylation (Wüstehube et al., 2010).

WT and p110α^D933A/WT mouse lung ECs (mLECs) showed no differences in DLL4-stimulated Akt phosphorylation (Fig. 5 A) and induction of the endogenous Notch target genes Hes1 and Hey1 (Fig. 5 B). In contrast, genetic interference with p110α activity dampened VEGF-A–induced mRNA expression of DLL4 in mLECs (Fig. 5 C). B16F1 tumors inoculated in p110α^D933A/WT mice, however, showed no or only slight reductions in the levels of DLL4 mRNA (Fig. 5 D) and protein (Fig. 5 E). This is most likely due to the fact that B16F1 cells produce DLL4 (Fig. 5 F), which masks the DLL4 present in the ECs. Upon systemic pharmacological inhibition of p110α, however, DLL4 levels in B16 tumors were severely reduced (Fig. 5 G), most likely because of a reduction in VEGF levels in the tumors (Fig. 1 S), together with inhibition

of DLL4 expression in both tumor cells and ECs. Collectively, these data indicate a possible involvement of reduced DLL4 levels in the nonfunctional angiogenesis induced by p110α PI3K inhibition. However, the phenotype observed upon p110α inhibition is only partially reminiscent of that observed upon Notch inhibition. Indeed, whereas Notch inhibition leads to a dramatic increase in EC numbers, blocking p110α activity in tumors results in reduced EC proliferation.

In summary, we report that inhibition of p110α in syngeneic mouse cancer models led to an increased density of smaller, hypoperfused vessels with altered vascular pericyte coverage, correlating with enhanced tumor hypoxia and tumor cell death. Although a consistent reduction of vessel size was observed upon p110α inhibition, the impact on the vessel number was more variable. However, it is clear that even when the number of vessel structures is increased, this does not rescue the reduced functionality of these small vessels. These observations suggest that the size of the vessels and not their number is the key parameter in the antiangiogenic effect of p110α inhibition. The impact of p110α in angiogenesis is most likely multifactorial, with reduction of DLL4 expression levels being only one aspect of its function, in addition to the regulation of EC proliferation, possibly in a Notch–independent manner. Strategies that confer sustained antiangiogenesis are expected to be essential for effective cancer therapy. The data presented here may offer an alternative to the vessel pruning strategies which are the mainstay of current antiangiogenic approaches.
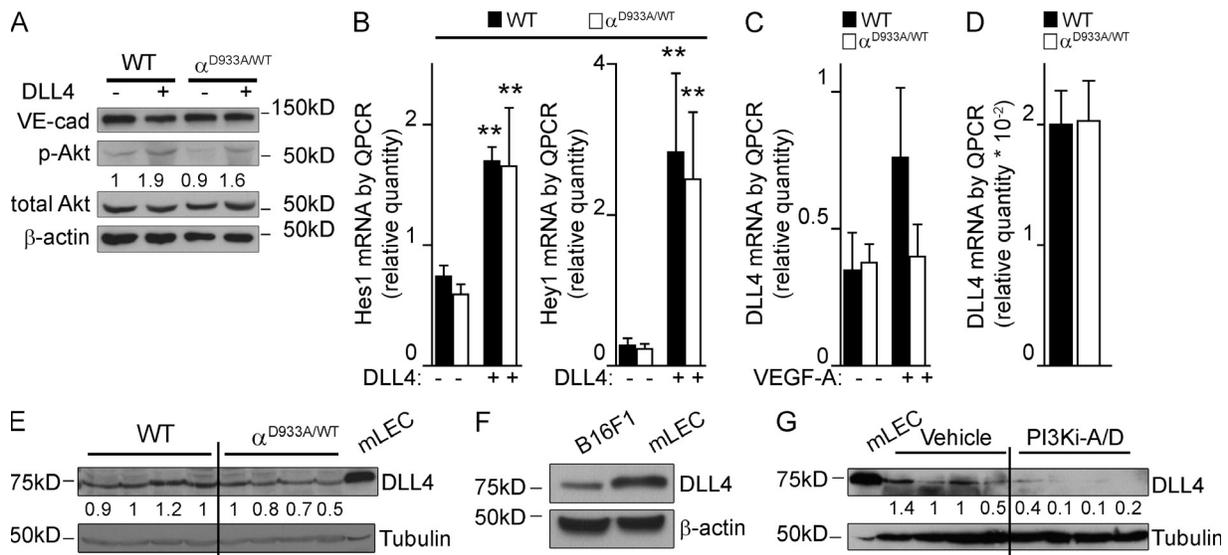
Figure 5. p110α inhibition reduces DLL4 levels in B16F1 tumors. (A) WT and p110α^D933A/WT mLECs were stimulated with DLL4 for 24 h, followed by immunoblotting of total cell lysate using the indicated antibodies (n = 3 for each genotype). (B) Hes1 and Hey1 mRNA levels in WT and p110α^D933A/WT mLECs stimulated with DLL4 (n ≥ 7 of each genotype). (C) DLL4 mRNA levels in WT and p110α^D933A/WT mLECs stimulated with VEGF-A (n = 6 of each genotype). (D) DLL4 mRNA levels in tumors inoculated in WT (n = 6) or p110α^D933A/WT (n = 7) mice. (E) DLL4 protein levels in tumors implanted in WT or p110α^D933A/WT mice. mLECs were used as a positive control. (F) DLL4 protein levels in cultured B16F1 cells and mLECs. (G) DLL4 protein levels in tumors from mice treated with vehicle or PI3Ki-A/D. mLECs were used as a positive control. (A, E, and G) Quantitation shows the relative immunoreactivity of each protein, normalized to the level of actin or tubulin.

MATERIALS AND METHODS

Mice. Mice were kept in individually ventilated cages and cared for according to the guidelines and legislation of the UK Home Office and Catalan Departament d'Agricultura, Ramaderia i Pesca, with procedures accepted by the Ethics Committees of Queen Mary University of London and IDIBELL-CEEA. All KI mice were backcrossed onto the C57/BL6 background for >10 generations and WT littermates used as controls. The C57/BL6 mice for pharmacological studies were obtained from Charles River UK.

Reagents. VEGF-165 (referred to as VEGF-A in the text) was purchased from PeproTech. Sources of antibodies were as follows: Cell Signaling Technology: Total Akt, pS473-Akt, and pSer240/244-S6; BD: CD31; NeoMarkers: Ki67; EMD Millipore: NG2 (AB5320); Abcam: desmin (ab15200); R&D: DLL4 (AF1389); Santa Cruz Biotechnology, Inc.: VE-cadherin (sc-6458); Sigma-Aldrich: α-SMA (C-6198), β-actin (A5441), and α-tubulin (T6074). All chemicals, unless otherwise stated, were purchased from Sigma-Aldrich. Secondary antibodies conjugated to Alexa Fluor 488 and Alexa Fluor 568 were obtained from Molecular Probes. PI3Ki-A/D and GDC-0941 were obtained from Genentech.

In vitro measurement of B16F1 cell proliferation and viability. B16F1 cells (10^5/well) were seeded onto 6-well plates 24 h before the addition of test compounds or vehicle (DMSO), followed by analysis of cell number and viability using an automatic cell counter, CASY model TT (Innovatis), 48 h later. LY294002 and PI3Ki-A/D were used at 10 μM and 0.3 μM, respectively.

Protein extraction and immunoblotting. B16F1 cells were plated in 60 cm² dishes at 0.5×10^6 cells per dish. 24 h later, cells were treated for 1 h with vehicle (DMSO), LY294002 (10 μM), PI3Ki-A/D (0.3 μM), or IC87114 (5 μM) and lysed in 50 mM Tris-HCl pH 7.4, 5 mM EDTA, 150 mM NaCl, 50 mM NaF and 1% Triton X-100 supplemented with 2 mg/ml aprotinin, 1 mM pepstatin, 1 ng/ml leupeptin, 1 mM phenylmethylsulfonylfluoride, and 1 mM sodium orthovanadate, followed by clearance of lysates by microcentrifugation. Supernatants were resolved on a 10% SDS-PAGE gel, transferred onto PVDF membranes, and probed with the indicated antibodies. Detection was performed by enhanced chemiluminescence.

Tumor studies in mice. Age- and sex-matched mice were given a single intradermal injection (50 μl) in the flank of 2×10^5 B16F1 or 5×10^5 CMT19T cells, followed by tumor isolation 2 wk later. For drug treatment, 8-wk-old WT females were given PI3Ki-A/D (75 mg/kg/day), GDC-0941 (100 mg/kg/day), or vehicle (0.5% (wt/vol) methylcellulose and 0.2% (wt/vol) polysorbate 80 in de-ionized water by oral gavage for 16 d. Drug administration started two days before tumor cell inoculation, and had no adverse impact on mouse viability and weight over the 16 d treatment period.

Histological analysis. Fresh tumor tissue was snap-frozen and cryosections made. Antibodies used for immunostaining were anti-CD31 (1:100), anti-Ki67 (1:50), anti-α-SMA (1:200), anti-NG2 (1:100), anti-desmin (1:150), pSer240/244-S6 (1:100). For immunofluorescence detection, Alexa Fluor 488 goat anti–rat IgG, Alexa Fluor 568 goat anti–rabbit IgG (H + L) and Alexa Fluor 568 goat anti–rat IgG were used at a dilution of 1:200. For nuclear counterstaining, DAPI (1:5,000) was added in the last PBS wash, followed by mounting of the sections in Mowiol. Blood vessel density and vessel area were quantified by counting the total number of CD31-positive vessels per field across the areas of viable tumor in each section (≥5 tumors/genotype and 4 images/tumor). Quantification of in vivo–proliferating tumor cells as assessed by the number of Ki67-positive cells relative to the number of DAPI-positive cells within the tumor of mice treated with vehicle was performed by counting 100 independent tumor cells per section. Coverage by mural cells is expressed as a percentage of vessels positive for α-SMA, NG2, or desmin per CD31-positive vessels.

Hypoxia in tissue was detected after intraperitoneal injection of 60 mg/kg pimonidazole, followed 1 h later by sacrifice of the mice by cervical dislocation.

Cryostat tissue sections were analyzed using a Hypoxyprobe Plus kit (Natural Pharmacia International Inc). For quantification purposes, only viable, non-necrotic areas (as determined by DAPI staining and assessment of altered nuclear morphology) of the tumor were considered.

Systemic perfusion of fluoresceinated lectin to visualize functional blood vessels was performed by injecting of 0.025 mg of fluorescence-labeled tomato lectin (FL-1171; Vector Laboratories) into the tail vein in a total volume of 50 μl. 3 min later, the mice were sacrificed by cervical dislocation, and tissue samples were prepared for OCT-embedded frozen sectioning. Tumor tissue was isolated and processed for immunostaining as described above. The number of lectin-perfused vessels and total number of vessels present in the entire viable area of each tumor section was counted.

Quantitative RT-PCR (qPCR) analysis. qPCR was performed using the following proprietary TaqMan Gene Expression assay FAM/TAMRA primers (Applied Biosystems): DLL4 (Mm00446968_m1), Hes1 (Mm01342805_m1), Hey1 (Mm00468865), and HPRT (Mm00446968_m1). The data show the $2^{-\Delta CT}$ values.

Measurement of VEGF. Exponentially growing B16F1 cells were incubated for 48 h with LY294002 (10 μM), PI3Ki-A/D (0.3 μM), IC87114 (5 μM), or vehicle. Medium was collected, centrifuged at 1,000 rpm for 5 min and VEGF concentration measured using a Quantikine Mouse VEGF immunoassay (R&D Systems) according to the manufacturer's instructions. This immunoassay was also used to measure VEGF in tumor extracts prepared by mincing tumors in 1 ml of PBS, followed by harvesting of the soluble fraction by centrifugation at 5,000 g for 5 min.

Isolation of ECs. Mouse lung ECs (mLECs) were isolated, purified, and cultured as previously described (Potente et al., 2007). In brief, mLECs were positively selected with anti–mouse vascular endothelial-cadherin (BD) antibody coated with magnetic beads (Invitrogen). Cells were cultured on gelatin-coated culture dishes in D-MEM/F12 supplemented with 20% fetal calf serum and endothelial cell growth factor (Promocell). After the first passage, the cells were repurified with vascular endothelial-cadherin antibody-coated magnetic beads.

Stimulation of mLECs. For DLL4 stimulation, mouse DLL4 (500 ng/ml) was immobilized by coating culture dishes for 1 h at 37°C, followed by seeding mLECs for 24 h. For stimulation with VEGF-A, mLECs were seeded in 6-well plates and starved in DMEM without FBS, and endothelial cell growth factor for 16 h, followed by stimulation with VEGF-A (200 ng/ml) for 2 h.

Statistical analysis. Statistical analysis was performed by nonparametric Mann Whitney's test or ANOVA test using Prism 5 (GraphPad Software Inc.). In all figures across the manuscript, errors bars are standard error of the mean. In all cases *, $P < 0.05$; **, $P < 0.01$; and ***, $P < 0.001$ were considered statistically significant.

REFERENCES

Armulik, A., G. Genové, and C. Betsholtz. 2011. Pericytes: developmental, physiological, and pathological perspectives, problems, and promises. *Dev. Cell.* 21:193–215. http://dx.doi.org/10.1016/j.devcel.2011.07.001

Chen, J., P.R. Somanath, O. Razorenova, W.S. Chen, N. Hay, P. Bornstein, and T.V. Byzova. 2005. Akt1 regulates pathological angiogenesis, vascular maturation and permeability in vivo. *Nat. Med.* 11:1188–1196. http://dx.doi.org/10.1038/nm1307

Díaz-Flores, L., R. Gutiérrez, J.F. Madrid, H. Varela, F. Valladares, E. Acosta, P. Martín-Vasallo, and L. Díaz-Flores Jr. 2009. Pericytes. Morphofunction, interactions and pathology in a quiescent and activated mesenchymal cell niche. *Histol. Histopathol.* 24:909–969.

Edgar, K.A., J.J. Wallin, M. Berry, L.B. Lee, W.W. Prior, D. Sampath, L.S. Friedman, and M. Belvin. 2010. Isoform-specific phosphoinositide 3-kinase inhibitors exert distinct effects in solid tumors. *Cancer Res.* 70:1164–1172. http://dx.doi.org/10.1158/0008-5472.CAN-09-2525

Foukas, L.C., M. Claret, W. Pearce, K. Okkenhaug, S. Meek, E. Peskett, S. Sancho, A.J. Smith, D.J. Withers, and B. Vanhaesebroeck. 2006. Critical role for the p110alpha phosphoinositide-3-OH kinase in growth and metabolic regulation. *Nature.* 441:366–370. http://dx.doi.org/10.1038/nature04694

Graupera, M., J. Guillermet-Guibert, L.C. Foukas, L.K. Phng, R.J. Cain, A. Salpekar, W. Pearce, S. Meek, J. Millan, P.R. Cutillas, et al. 2008. Angiogenesis selectively requires the p110alpha isoform of PI3K to control endothelial cell migration. *Nature.* 453:662–666. http://dx.doi.org/10.1038/nature06892

Herbert, S.P., J. Huisken, T.N. Kim, M.E. Feldman, B.T. Houseman, R.A. Wang, K.M. Shokat, and D.Y. Stainier. 2009. Arterial-venous segregation by selective cell sprouting: an alternative mode of blood vessel formation. *Science.* 326:294–298. http://dx.doi.org/10.1126/science.1178577

Hirschi, K.K., and P.A. D'Amore. 1997. Control of angiogenesis by the pericyte: molecular mechanisms and significance. *EXS.* 79:419–428.

Lelievre, E., P.M. Bourbon, L.J. Duan, R.L. Nussbaum, and G.H. Fong. 2005. Deficiency in the p110alpha subunit of PI3K results in diminished Tie2 expression and Tie2(-/-)-like vascular defects in mice. *Blood.* 105:3935–3938. http://dx.doi.org/10.1182/blood-2004-10-3955

Liu, Z.J., T. Shirakawa, Y. Li, A. Soma, M. Oka, G.P. Dotto, R.M. Fairman, O.C. Velazquez, and M. Herlyn. 2003. Regulation of Notch1 and Dll4 by vascular endothelial growth factor in arterial endothelial cells: implications for modulating arteriogenesis and angiogenesis. *Mol. Cell. Biol.* 23:14–25. http://dx.doi.org/10.1128/MCB.23.1.14-25.2003

Nasarre, P., M. Thomas, K. Kruse, I. Helfrich, V. Wolter, C. Deppermann, D. Schadendorf, G. Thurston, U. Fiedler, and H.G. Augustin. 2009. Host-derived angiopoietin-2 affects early stages of tumor development and vessel maturation but is dispensable for later stages of tumor growth. *Cancer Res.* 69:1324–1333. http://dx.doi.org/10.1158/0008-5472.CAN-08-3030

Noguera-Troise, I., C. Daly, N.J. Papadopoulos, S. Coetzee, P. Boland, N.W. Gale, H.C. Lin, G.D. Yancopoulos, and G. Thurston. 2006. Blockade of Dll4 inhibits tumour growth by promoting non-productive angiogenesis. *Nature.* 444:1032–1037. http://dx.doi.org/10.1038/nature05355

Okkenhaug, K., A. Bilancio, G. Farjot, H. Priddle, S. Sancho, E. Peskett, W. Pearce, S.E. Meek, A. Salpekar, M.D. Waterfield, et al. 2002. Impaired B and T cell antigen receptor signaling in p110delta PI 3-kinase mutant mice. *Science.* 297:1031–1034.

Phung, T.L., K. Ziv, D. Dabydeen, G. Eyiah-Mensah, M. Riveros, C. Perruzzi, J. Sun, R.A. Monahan-Earley, I. Shiojima, J.A. Nagy, et al. 2006. Pathological angiogenesis is induced by sustained Akt signaling and inhibited by rapamycin. *Cancer Cell.* 10:159–170. http://dx.doi.org/10.1016/j.ccr.2006.07.003

Potente, M., L. Ghaeni, D. Baldessari, R. Mostoslavsky, L. Rossig, F. Dequiedt, J. Haendeler, M. Mione, E. Dejana, F.W. Alt, et al. 2007. SIRT1 controls endothelial angiogenic functions during vascular growth. *Genes Dev.* 21:2644–2658. http://dx.doi.org/10.1101/gad.435107

Qayum, N., R.J. Muschel, J.H. Im, L. Balathasan, C.J. Koch, S. Patel, W.G. McKenna, and E.J. Bernhard. 2009. Tumor vascular changes mediated by inhibition of oncogenic signaling. *Cancer Res.* 69:6347–6354.

Qayum, N., J.H. Im, M.R. Stratford, E.J. Bernhard, W.G. McKenna, and R.J. Muschel. 2012. Modulation of the tumor microvasculature by phosphoinositide-3 kinase inhibition increases doxorubicin delivery in vivo. *Clin. Cancer Res.* 18:161–169.

Ridgway, J., G. Zhang, Y. Wu, S. Stawicki, W.C. Liang, Y. Chanthery, J. Kowalski, R.J. Watts, C. Callahan, I. Kasman, et al. 2006. Inhibition of Dll4 signalling inhibits tumour growth by deregulating angiogenesis. *Nature.* 444:1083–1087. http://dx.doi.org/10.1038/nature05313

Rodon, J., R. Dienstmann, V. Serra, and J. Tabernero. 2013. Development of PI3K inhibitors: lessons learned from early clinical trials. *Nat Rev Clin Oncol.* 10:143–153. http://dx.doi.org/10.1038/nrclinonc.2013.10

Schmid, M.C., C.J. Avraamides, H.C. Dippold, I. Franco, P. Foubert, L.G. Ellies, L.M. Acevedo, J.R. Manglicmot, X. Song, W. Wrasidlo, et al. 2011. Receptor tyrosine kinases and TLR/IL1Rs unexpectedly activate myeloid cell PI3kγ, a single convergent point promoting tumor inflammation and progression. *Cancer Cell.* 19:715–727. http://dx.doi.org/10.1016/j.ccr.2011.04.016

Takeshita, K., M. Satoh, M. Ii, M. Silver, F.P. Limbourg, Y. Mukai, Y. Rikitake, F. Radtke, T. Gridley, D.W. Losordo, and J.K. Liao. 2007. Critical role of endothelial Notch1 signaling in postnatal angiogenesis. *Circ. Res.* 100:70–78. http://dx.doi.org/10.1161/01.RES.0000254788.47304.6e

Wüstehube, J., A. Bartol, S.S. Liebler, R. Brütsch, Y. Zhu, U. Felbor, U. Sure, H.G. Augustin, and A. Fischer. 2010. Cerebral cavernous malformation protein CCM1 inhibits sprouting angiogenesis by activating DELTA-NOTCH signaling. *Proc. Natl. Acad. Sci. USA.* 107:12640–12645. http://dx.doi.org/10.1073/pnas.1000132107

Yuan, T.L., H.S. Choi, A. Matsui, C. Benes, E. Lifshits, J. Luo, J.V. Frangioni, and L.C. Cantley. 2008. Class 1A PI3K regulates vessel integrity during development and tumorigenesis. *Proc. Natl. Acad. Sci. USA.* 105:9739–9744. http://dx.doi.org/10.1073/pnas.0804123105

Zhao, J.J., H. Cheng, S. Jia, L. Wang, O.V. Gjoerup, A. Mikami, and T.M. Roberts. 2006. The p110alpha isoform of PI3K is essential for proper growth factor signaling and oncogenic transformation. *Proc. Natl. Acad. Sci. USA.* 103:16296–16300. http://dx.doi.org/10.1073/pnas.0607899103